

SORPTION EFFICIENCY OF CO₂ BY FUNCTIONALIZED CHITOSAN BIOFILMS AS A GREENHOUSE GAS EMISSION CONTROL SYSTEM

X. Galindo^a, J. Benitez ^{a,b*}, L. Tuguez ^a

^a Environmental Engineering Department, Universidad Católica Andrés Bello, Caracas, Venezuela.

^b Environmental Sustainability Department, Universidad Católica Andrés Bello, Caracas, Venezuela

* Correspondence author, E-mail: jbenitez@ucab.edu.ve, phone +58 414 6108128 Fax +58 212 4076059

Received: 07-03-2024
Published: 07-06-2024

Accepted: 06-06-2024

ABSTRACT

The accumulation of greenhouse gases inevitably affects the temperature of both the atmosphere and the Earth's surface, standing as a primary driver of global climate change. The atmospheric concentration of CO₂, a greenhouse gas, has risen from a pre-industrial level (mid-18th century) of 280 ppmv to the current 421 ppmv, with an annual increase of approx. 1.8 ppmv. Using chitosan biofilms, a naturally occurring cationic polysaccharide, as a CO₂ sorbent presents an economically viable alternative. Chitosan can be sourced from waste in the fishing industry, and its low toxicity and biodegradability make it easy to handle and recycle. In this context, the main goal of this research is to assess the CO₂ sorption efficiency of amines-functionalized chitosan biofilms in batch injection systems, along with their characterization through Scanning Electronic Microscopy (SEM) and thermal stability analysis using DSC. The findings of this study reveal that chitosan films exhibit high thermal stability (215°C) and a remarkable CO₂ sorption capacity (3.76 mmol CO₂/g film). Moreover, the immobilization of basic groups (tetraethylenepentamine – TEPA and polyethylenimine - PEI) through impregnation enhances the CO₂ fixation capacity, even at elevated temperatures, underscoring the significant potential of these materials for controlling CO₂ emissions.

Keywords: biopolymer; chitosan; chitin; sorption; carbon dioxide.

Eficiencia de sorción de CO₂ de biopolímeros funcionalizados de quitosano como sistema de control de emisión de gases de efecto invernadero

RESUMEN

La acumulación de gases de efecto invernadero inevitablemente influye en la temperatura de la atmósfera y de la superficie terrestre, siendo una de las principales causas del cambio climático global. La concentración atmosférica de CO₂, el cual es un gas de efecto invernadero, ha aumentado desde un valor pre-industrial (mediados del siglo XVIII) de 280 ppmv hasta los actuales 421 ppmv con un incremento de aprox. 1,8 ppmv/año. El empleo de biopelículas de quitosano, un polisacárido catiónico natural, como sorbente de CO₂, representa una opción económica alternativa, ya que el mismo puede ser obtenido a partir de desechos de la industria pesquera, además que su baja toxicidad y biodegradabilidad facilita su manejo y reciclabilidad. En este sentido, este trabajo tiene como objetivo fundamental evaluar la eficiencia de sorción de CO₂ de biopelículas de quitosano funcionalizado con aminas en sistemas de inyección por carga y su caracterización por microscopía electrónica de barrido (SEM) y estabilidad térmica por DSC. De esta investigación, se concluye que las películas de quitosano poseen una alta estabilidad térmica (215°C) y moderada capacidad de adsorción de CO₂ (3,76 mmol CO₂/g película). La inmovilización de grupos básicos (tetraetilenpentamina - TEPA y polietilenimina - PEI) por impregnación mejora la capacidad de fijación de CO₂, incluso a altas temperaturas, lo que demuestra el gran potencial de aplicación que tienen estos materiales como sistema de control de emisión de CO₂.

Palabras clave: biopolímero, quitosano, quitina, sorción, CO₂.

INTRODUCTION

The accumulation of greenhouse gases inevitably influences the temperature of the atmosphere and the Earth's surface. Oxygen, nitrogen, water, carbon dioxide, and ozone molecules are nearly transparent to solar radiation, but molecules such as CO₂, H₂O, O₃, CH₄, NO₂, perfluorocarbons (PFC), hydrofluorocarbons (HFC), and HFS₆ are partially opaque to infrared radiation. In other words, they absorb the radiation emitted by the ground that has been previously heated by solar radiation. When infrared radiation strikes CO₂, H₂O, O₃, CH₄, and fluorocarbon molecules, it is absorbed by them. These molecules vibrate and re-emit infrared energy, causing the phenomenon known as the greenhouse effect, which keeps the Earth's atmosphere warm [1].

Additionally, CO₂ absorbs 71% of long-wave radiation (FTIR, $\lambda = 13\text{-}17.5\ \mu\text{m}$) emitted by the Earth, releasing it into the atmosphere in the form of heat. However, if its concentration increases, the atmosphere provides greater resistance to the necessary escape of radiation into space. As a result, the temperature of the Earth's surface rises due to the increased rate of radiation absorbed, ranging from 161 to 333 W/m². This warming will lead to increased evaporation of water from the oceans. Water vapor acts as the most potent greenhouse gas, at least in the very short term, amplifying the warming effect.

The concentration of carbon dioxide (CO₂) in the atmosphere has increased significantly since the onset of the Industrial Era, rising from approximately 278 parts per million (ppm) in 1750 to 414.7 ± 0.1 ppm in 2021 [2]. This rise in atmospheric CO₂ levels is primarily attributed to human activities, particularly the release of carbon from deforestation and changes in land use [3]. Global fossil CO₂ emissions, which include emissions from fossil fuel combustion and cement production, continued to rise in 2022, surpassing pre-COVID-19 pandemic levels seen in 2019. In 2021, emissions

increased by 0.46 GtC yr⁻¹ (equivalent to 1.7 GtCO₂ yr⁻¹), reaching 9.9 ± 0.5 GtC yr⁻¹ (36.3 ± 1.8 GtCO₂ yr⁻¹), matching the levels observed in 2019. Preliminary estimates indicate that fossil CO₂ emissions further increased by approximately 1.1% in 2023 relative to 2022, reaching 10.0 Gt C yr⁻¹ (36.8 Gt CO₂ yr⁻¹) slightly exceeding the levels recorded in 2019 [4]. Without the implementation of effective policies to mitigate emissions, projections suggest that energy-related greenhouse gas emissions, primarily from fossil fuel combustion, could increase by 50% from 38 Gt of CO₂ in 2004 to 57 Gt of CO₂ in 2030, posing significant challenges for mitigation efforts.

Currently, there are various approaches that can contribute to reducing CO₂ emissions in many power plants. One of them is to develop innovative and cost-effective CO₂ capture technologies that are scalable to the required size for both energy and non-energy sectors. The purpose of capture is to produce a concentrated stream of CO₂ at high pressure that can be easily transported to a storage location. Current processes use aqueous solutions of 20-30% weight MEA for post-combustion CO₂ capture. However, this process requires a significant amount of energy in the amine regeneration stage. Additionally, thermal and oxidative degradation of solvents results in a high solvent replenishment rate and the production of compounds that are highly toxic and corrosive [5].

In this context, chitosan-based adsorbent films are considered a viable option for post-combustion CO₂ capture due to their biodegradability, biorenewability, biocompatibility, physiological inertness, and hydrophilicity [6]. Chitosan is a natural polymer resulting from the N-deacetylation of chitin, the second most abundant natural polymer after cellulose, with a global estimated production of approximately 10¹¹ tons per year [7]. Chitin is present in fungi, diatoms, nematodes,

arthropods, and many animals and plants. Additionally, shells of shrimp, crabs, lobsters, as well as squid waste from the marine processing industry have become the main resources used today to produce chitosan [8].

Approximately 70% of marine capture fishing is used for processing, and a significant amount of the remaining catch becomes waste [9]. The discarded material exceeds 20 million tons annually, equivalent to 25% of the total annual production. In crustaceans, the waste constitutes 45% by weight of mollusks and includes discarded heads, thoraxes, legs, and shells. These chitinous seafood wastes are considered hazardous due to their highly perishable nature and contaminating effect if disposed of offshore [10]. This has led to the conversion of fishery waste into high-value products such as fish and pet food, fertilizers, and possibly as solid CO₂ adsorbents [11].

To date, research in using biopolymers as a support for the dispersion of active amino groups for CO₂ adsorption is in its early stages. Ito et al. were among the pioneering groups to demonstrate the potential of chitosan as a selective membrane for CO₂ separation [12]. They observed that a chitosan membrane, when swollen by water vapor in the feed gas, exhibited significant gas permeability. Specifically, carbon dioxide showed preferential permeation through the swollen chitosan membrane, with a permeability of $2.5 \times 10^{-8} \text{ cm}^3 \text{ (STP) cm (s cm}^2 \text{ cmHg)}^{-1}$ and a CO₂/N₂ separation factor of 70 at room temperature. Pristine chitosan exhibits relatively low adsorption capacity for CO₂ (0.47 mmol/g) [13]. However, the development of chitosan-based composites, such as chitosan/SiO₂ nanoparticles (4.39 mmol/g) [14] and chitosan/zeolite (1.7 mmol/g) [15] has led to improved adsorption capacities compared to pristine chitosan. While pure chitosan membranes may exhibit lower CO₂ separation performance compared to blends due to fewer active carriers [16], they still offer advantages over existing polymeric membranes due to

facilitated transport mechanisms rather than just solution diffusion [17, 18]. El-Azami's group has conducted extensive research using dry chitosan [19], swollen chitosan [20] and amine-blended chitosan membranes [21], highlighting the hydrophilic nature of chitosan membranes in achieving superior CO₂ separation performance from gases such as N₂ and H₂. However, chitosan has limitations, including acid solubility, which can be addressed through structural modifications or blending with other materials.

This study aims to evaluate the CO₂ sorption efficiency of amino-functionalized chitosan films in batch injection systems. For this purpose, functionalized chitosan films were prepared through acid gelation, followed by ionic cross-linking reactions and amino group anchoring by impregnation. The chitosan films were characterized using Fourier-transform infrared spectroscopy (FTIR) and Scanning Electron Microscopy (SEM). The effect of the degree of ionic cross-linking on the thermal stability of the chitosan film was studied using thermogravimetric analysis (TGA) and differential scanning calorimetry (DSC). Additionally, the effect of various functionalizing agents (extended amine systems) and the temperature of the batch injection system on the CO₂ sorption capacity of the synthesized chitosan films was evaluated.

MATERIAL AND METHODS

Synthesis of Chitosan Films.

The chitosan flakes used for the synthesis of the films were provided by the company INNOVAQUITO with a deacetylation degree of 95%. The cross-linking agent used was Merck Sodium Citrate CAS 6132-04-3, which did not require additional purification. To obtain biopolymer films, the acid gelation method proposed by Silva et al. was followed [22]. Initially, a chitosan solution was prepared by dissolving a portion of 95% DA chitosan flakes in 300 mL of 2% v/v acetic acid solution

(Honeywell Brand, CAS 64-19-7). The solution was mechanically stirred at a constant speed for 4 hours, then vacuum-filtered using a Leybold-Trivac pump to remove any insoluble suspended solids. Once the solution was completely homogeneous, a portion of the chitosan solution was poured into a Petri dish and placed in an oven at 40°C for 24 hours.

Cross-linking process of chitosan films.

The ionic cross-linking procedure was carried out by immersing the biopolymer films in a solution with sodium citrate concentrations of 10% and 40% w/v for 24 hours (without pH adjustment). Subsequently, the films were removed from the system and washed thoroughly with water. The cross-linked film was then air-dried at room temperature for 24 hours. (See Figure 1).

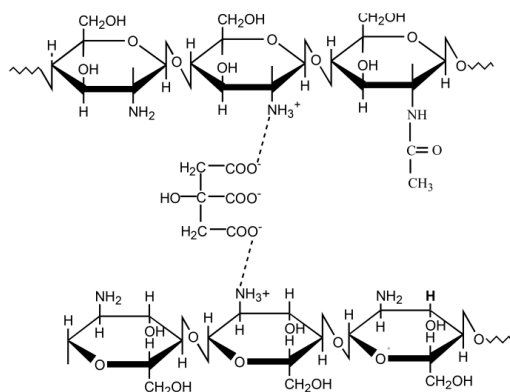


Fig. 1. Structure of chitosan membranes ionically cross-linked with sodium citrate.

Functionalization of chitosan films by wet impregnation.

The functionalization by impregnation was carried out by immersing the cross-linked chitosan film in a flask containing a solution formed by the amine dissolved in ethanol (e.g., 1 g of tetraethylenepentamine - TEPA or polyethylenimine - PEI + 10 g of ethanol) (Tetraethylenepentamine Merck CAS 112-57-2 and Branched Polyethylenimine CAS 9002-98-6). The mixture was then placed in an oven at 40°C for 24 hours to slowly evaporate the ethanol from the solution. The

impregnated film was subsequently vacuum-dried for 3 hours in a flask equipped with a stopcock and using a Leybold-Trivac vacuum pump.

Characterization by FTIR spectroscopy of the cross-linked and functionalized chitosan films was performed in the FTIR range of 400-4000 cm^{-1} with 50 spectral scans and a resolution of 2 cm^{-1} to determine the presence of amino groups and verify the cross-linking of chitosan film. Thermo NICOLET 6700 equipment was used for this purpose. Dry KBr pellets were prepared in a ratio of 1:10 following the ASTM E1252-98 [23]. Morphological and topographic information about the surface of the films was obtained by Scanning Electronic Microscopy (SEM) using a Hitachi, Ltd. S-400 Field Emission Scanning Electron Microscope. Energy Dispersive X-ray Spectroscopy (EDX) analysis, frequently coupled with scanning electron microscopy, facilitated the quantitative assessment of the chemical composition of surface film and thus to determine the proportion of nitrogen introduced into the biopolymer via impregnation. For thermogravimetric studies, approximately 10 mg of the functionalized biopolymer sample was taken and placed in the thermobalance, heating in a temperature range from 30°C to 600°C with a heating rate of 5 degrees/min and a nitrogen flow of 20 mL/min using Pyris 6 TGA Perkin Elmer equipment following ASTM E1131-08 [24].

Sorption Capacity Measurement.

Sorption capacity tests for chitosan films were conducted in an autoclave (cylindrical batch-type reactor), consisting of a stainless-steel vessel capable of withstanding pressures up to $2,068 \times 10^7$ Pa and a maximum temperature of 350°C. The Anton-Paar autoclave comprised a 100 ml vessel, a lid with gas inlet and outlet connections, a pressure gauge, a connector attached to a Parr 4843 pressure transmitter coupled to an interface recording the system pressure over time, and a

thermocouple for recording the system temperature, also connected to the same interface. To analyze the effect of functionalizing and cross-linking agents on sorption capacity, the previously described capture test was conducted at three different temperatures (room, 50°C, and 80°C) with 413,7 kPa partial CO₂ pressure, varying the type of evaluated functionalized films. The adsorption capacity of the chitosan film was calculated using the initial and final pressure method [25]. This method involves reporting the mass of sorbed gas (CO₂, calculated using the Ideal Gas Law) relative to the mass of the chitosan film used.

Table I. Calibration range and resolution of pressure and temperature measuring and transmitters devices.

Device	Measuring range	Reading Error
Temperature transmitter	0,000 – 750,000 °C	± 0,0001 °C
Pressure transmitter	0,000 – 1,38 x10 ⁷ Pa	± 0,0001 Pa
Autoclave manometer	0 – 690 kPa	± 34,5 kPa

RESULTS AND DISCUSSION

Characterization results

Chitosan exhibits important FTIR spectral regions: (1) area between 3000 and 3300 cm⁻¹ assigned to free or interacting hydroxyl groups and amino groups; (2) region between 2850 and 2950 cm⁻¹ for alkyl chains (-CH₂-); (3) the zone between 1650 and 1750 cm⁻¹ associated with carbonyl (-C=O) and amide (-C-N) groups; and (4) the region around 1000 cm⁻¹ where FTIR bands of the C-O glycosidic bonds can be observed, which act as a linkage bridge between the monomers forming chitosan.

The FTIR spectra of the unmodified chitosan membrane and the chitosan membrane cross-linked with sodium

citrate (NaCit) are shown in Figures 2a and 2b, respectively. In both the cross-linked and unmodified films, an absorption band at 1636 cm⁻¹ is observed, which can be attributed to the N-H deformation vibration of the NH³⁺ ion. Additionally, the FTIR spectrum of the membrane ionically cross-linked with NaCit shows a strong and well-defined band around 1375 cm⁻¹ associated with the C-O bending vibration of the carboxylate ion (COO⁻) from the cross-linking agent. All these spectral changes indicate the cross-linking reaction between the protonated amino groups of chitosan and the carboxylate groups of sodium citrate.

Figure 2c displays the FTIR spectrum of the 1% NaCit cross-linked chitosan film impregnated with the polymeric amine, polyethyleneimine. Spectral changes observed in the infrared region for the modified membrane include: (a) an increase in the intensity of signals in the region of 3300-3200 cm⁻¹ (from an absorbance of 1.14 to 1.25), associated with N-H stretching vibrations and their interaction through hydrogen bonds with the hydroxyl groups of the membrane; (b) an intensity increase of the band around 1560 cm⁻¹ due to the N-H deformation vibration of the primary amine, which is overlapped with the amide II band at the same wavenumber; and (c) an increase in the intensity of signals at 2835 cm⁻¹ and the band at 1463 cm⁻¹ corresponding to stretching and deformation of the C-H bond of the CH₂ group, respectively. Both changes are generated by the increase in methylene groups of the membranes, which come from the incorporated polymeric amine.

A further modification to the cross-linking of chitosan films involves their wet impregnation with an aliphatic amine such as tetraethylenepentamine. Figure 2d shows the infrared spectrum of the 1% NaCit cross-linked film that was impregnated with tetraethylenepentamine. The increase of basic groups in the membrane structure is

evident by the enhanced intensity of the FTIR signal in the region from 3400 to 3200 cm^{-1} (with an absorbance of approximately 1.47) compared to the unimpregnated film band (with an absorbance of 1.14). This enhancement is associated with the stretching vibrations of N-H and its interaction with intra- and intermolecular hydrogen bonds.

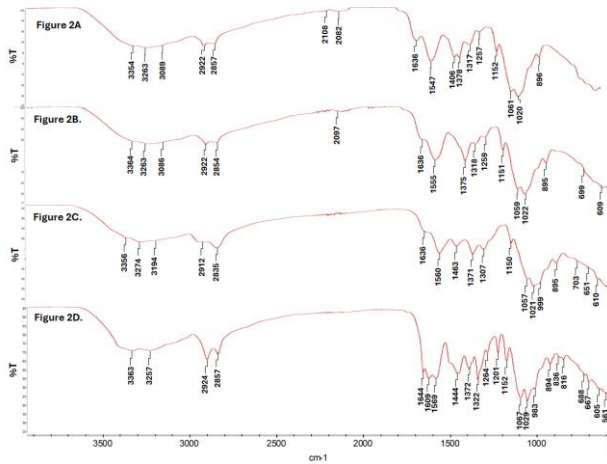


Fig. 2. Infrared spectrum 2A: Chitosan film; 2B: Chitosan film cross-linked with 1% sodium citrate; 2C: Chitosan film cross-linked with 1% NaCit and impregnated with polyethyleneimine (PEI); 2D: Chitosan film cross-linked with 1% NaCit and impregnated with 2% tetraethylenepentamine (TEPA).

Scanning electron microscopy characterization

Figure 3a shows the micrographs obtained from the unmodified chitosan film, where a highly homogeneous surface without defined porosity is observed. In the magnified micrographs (12,000x and 1,608x), regular folds with a moderate level of roughness are visible. According to the magnified micrographs, the surface of the chitosan film exhibits randomly distributed microstructured spaces, suggesting the existence of surface fissures. This type of morphological detail indicates that the particles in the chitosan films may have some crystallization flaws associated with the short

gelification period resulting from a rapid volatilization of the solvent.

However, when the films undergo cross-linking with sodium citrate, a change in surface topology is observed. In Figure 3b, the membranes exhibit smooth and regular edges, a result of the cross-linking of the chitosan chains. Additionally, a more ordered and compact surface is defined within a range of 100 μm compared to the unmodified chitosan films.

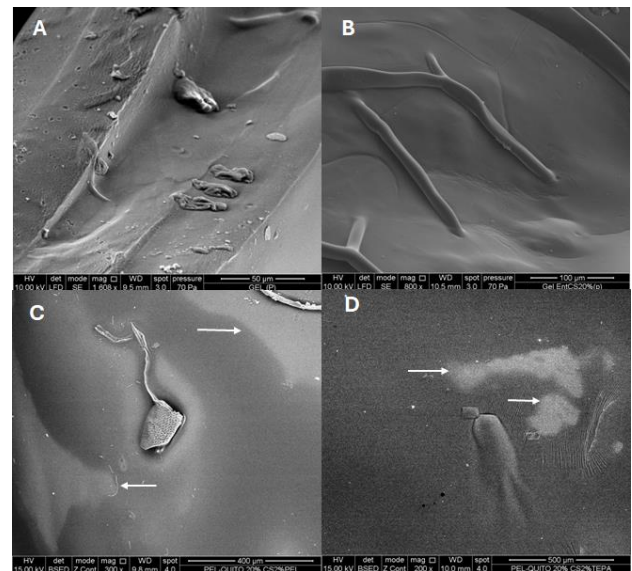


Fig. 3. Micrographs: (3A): Unmodified chitosan films; (3B): Chitosan films cross-linked with a 20% sodium citrate solution; (3C): Chitosan films cross-linked with 20% sodium citrate and impregnated with 2% polyethyleneimine; (3D): Chitosan films cross-linked with 20% sodium citrate and impregnated with 2% tetraethylenepentamine.

Furthermore, some macroscopic changes in the membranes occur, including a color shift from pale yellow to transparent and increased resistance to fracture or mechanical disintegration. The multitude of inter- and intramolecular hydrogen bonds, coupled with ionic cross-linking, robustly stabilize the structural arrangement of chitosan molecules across all three dimensions of the unit

cell. This alteration in intramolecular order or short-range crystallinity dictates the presence of a denser and more uniform microstructural configuration.

The Scanning Electronic Microscopy (SEM) images of films impregnated with tetraethylenepentamine and polyethyleneimine in ethanol (See Figure 3c and 3d) reveal a heterogeneous incorporation of the amine on the surface of the chitosan film. The arrows in Figure 3c and 3d indicate areas with a large deposit of amino groups in contrast to darker areas with lower impregnation. The lack of homogeneity in the immobilization of the amine on the chitosan membrane may be associated with the presence of folds and surface irregularities inherent to the membrane, reducing the exposed area of the film for functionalization.

Thermogravimetric analysis

The thermogram of the chitosan film exhibits three thermal events with weight losses of 8.7%, 5.2%, and 40.8%, respectively, which are related to the loss of free water at 85.4°C, combined water at 212.2°C, and thermodegradation at 290.2°C (See Figure 4A). The mechanism of thermal depolymerization of the chitosan film is based on the interaction between the protonated amine and the glucosidic bond. After the protonation of the glucosidic bonds, hydrolysis occurs when protonated glucosidic bond reacts with water. According to Nieto et al., the pyrolysis process of polysaccharides initiates with the random cleavage of glucosidic bonds (C-O-C), followed by the decomposition and generation of acetic and butyric acids, along with a spectrum of lower fatty acids, where C₂, C₃, and C₆ are predominant [26].

The thermal stability of the amine incorporated in the chitosan film is a crucial property to consider, as degradation of the amine can occur during cyclic CO₂ capture tests. As shown in Figure 4B, the thermogram of the chitosan film crosslinked with 1% NaCit and

impregnated with 2% tetraethylenepentamine exhibits four weight loss regions. The first, at a temperature of 100.1°C is due to the desorption of pre-adsorbed CO₂ and physically absorbed residual water. The weight loss in the first endothermic peak of the tetraethylenepentamine-loaded film (13.33%) is higher compared to the mass change recorded for the film incorporating polyethylenimine (8.28%) (See Figure 4C). This reflects the higher affinity of the tetraethylenepentamine - impregnated film for moisture and CO₂, explaining the higher CO₂ sorption capacity, a behavior that will be described in subsequent sections.

The second region involves the gradual evaporation of the amine (tetraethylenepentamine -TEPA) with a dramatic decrease in weight loss (29.67%) at temperatures between 150°C to 290°C. Based on the thermal stability results of Hyun et al., liquid tetraethylenepentamine (TEPA) exhibits the same thermal behavior, with a degradation zone starting at 150°C and extending up to 260°C [27]. A third exothermic event corresponds to the decomposition and depolymerization of the chitosan film with a mass loss of 20.16% and a temperature of maximum degradation rate of 316.5°C, making the impregnated film slightly more thermally stable than the unmodified one. The last stage of the thermogravimetric profile is located at temperatures above 350°C, which can be attributed to the decomposition of residual organic groups.

The thermal stability of the film impregnated with polyethylenimine (PEI) in nitrogen up to approximately 600°C is presented in Figure 4C. The first mass loss of the impregnated film is around 8.28% occurring at 89.3°C. This can be attributed to adsorbed moisture, i.e., free water, while the removal of combined water is suggested to occur in a second thermal event at 236.3°C, equivalent to a weight loss of 5.93%. It is also possible that slow volatilization of polyethylenimine (PEI) occurs

at these temperatures. Above 260°C, there is a drastic decrease in weight with a percentage loss of 18.35%, because of the volatilization and/or pyrolysis of polyethyleneimine. The depolymerization and decomposition of the chitosan film occur at 374.4°C with a mass loss of 36.77%. This temperature is higher compared to the non-impregnated film (307.6°C).

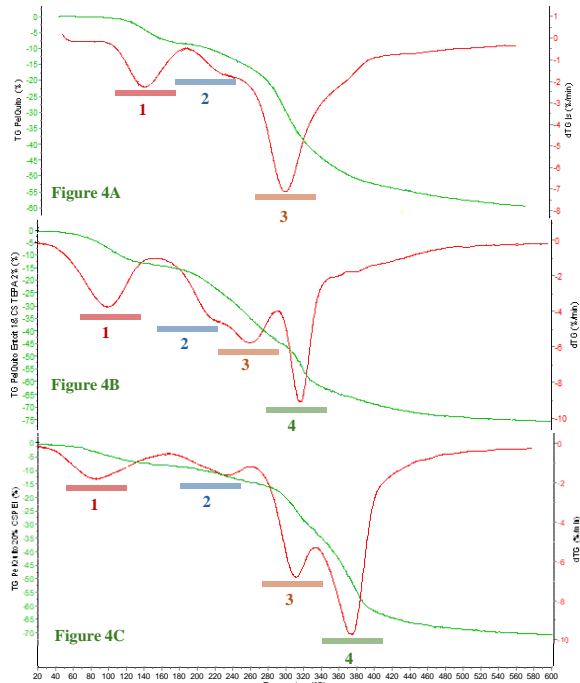


Figure 4A

Stage	TG Parameter			DTG Parameter		
	Initial Temperature (°C)	Final Temperature (°C)	Weight Loss (Δm, %)	Initial Temperature (°C)	Final Temperature (°C)	Peak Maximum (°C)
1	23,38	147,21	8,74	25,11	147,21	85,4
2	147,21	222,4	5,23	146,81	212,22	212,2
3	223,11	452,57	40,797	212,22	455,79	290,2

Figure 4B

Stage	TG Parameter			DTG Parameter		
	Initial Temperature (°C)	Final Temperature (°C)	Weight Loss (Δm, %)	Initial Temperature (°C)	Final Temperature (°C)	Peak Maximum (°C)
1	26,26	152,63	13,33	24,11	152,88	100,1
2	151,28	289,98	29,67	152,2	225,31	225,3
3	291,11	354,16	20,16	225,31	291,05	260,1
4	353,93	588,09	11,7	290,51	373,87	316,5

Figure 4C

Stage	TG Parameter			DTG Parameter		
	Initial Temperature (°C)	Final Temperature (°C)	Weight Loss (Δm, %)	Initial Temperature (°C)	Final Temperature (°C)	Peak Maximum (°C)
1	26,11	171,05	8,28	31,98	170,5	89,3
2	171,8	263,03	5,93	171,11	263,09	236,3
3	263,77	334,55	18,35	263,09	334,41	312,7
4	335,38	547,78	36,77	334,32	544,28	374,4

Fig. 4. Thermal analysis, TGA (green curve), DTG (red curve), 4A: Chitosan film; 4B: Chitosan film crosslinked with 1% sodium citrate and impregnated with 2% tetraethylenepentamine (TEPA); 4C: Chitosan film

crosslinked with 1% sodium citrate and impregnated with 2% polyethyleneimine (PEI).

Examining the DSC curve of the uncrosslinked film reveals a narrower and more symmetric first endothermic signal around 77.7°C compared to the endothermic peak exhibited by the film crosslinked with 1% NaCit and impregnated with 2% TEPA (See Figure 5A and 5B). This discrepancy stems from a higher concentration of incorporated amino groups within the film relative to the hydroxyl groups present in the glucosidic rings.

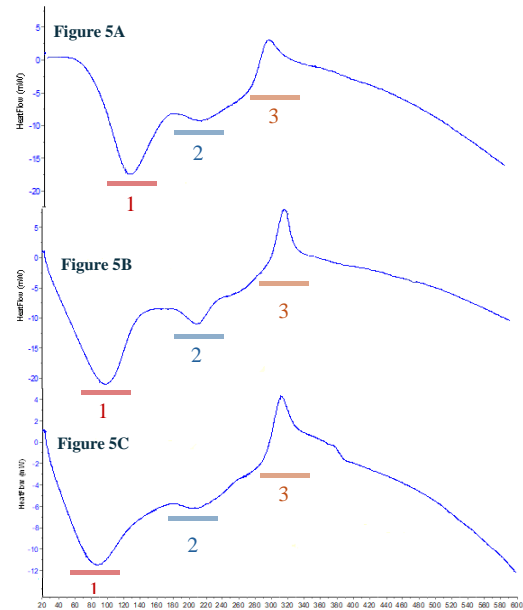


Figure 5A

Stage	DSC Parameter			
	Initial Temperature (°C)	Final Temperature (°C)	Heat (J/g)	Peak Maximum (°C)
1	23,41	152,68	326,96	77,7
2	154,6	237,0	22,28	193,1
3	237,81	350,86	-69,8	286,8

Figure 5B

Stage	DSC Parameter			
	Initial Temperature (°C)	Final Temperature (°C)	Heat (J/g)	Peak Maximum (°C)
1	23,95	172,43	414,96	93,4
2	172,3	254,4	35,4	214,7
3	287,43	354,68	-49,33	319,9

Figure 5C

Stage	DSC Parameter			
	Initial Temperature (°C)	Final Temperature (°C)	Heat (J/g)	Peak Maximum (°C)
1	23,23	153,07	215,28	73,2
2	153,56	264,72	45,70	206,3
3	267,7	350,54	-56,092	310,53

Fig. 5. Differential calorimetric analysis (DSC), (5A): Chitosan film; (5B): Chitosan film crosslinked with 1% sodium citrate and impregnated with 2% TEPA; (5C):

Chitosan film crosslinked with 1% sodium citrate and impregnated with 2% PEI.

In this context, due to the differing water affinity towards hydroxyl and amino groups, water molecule release predominantly occurs via weaker interactions with hydroxyl groups. During heating, thermally activated water molecules tend to desorb, with those bound to amino groups liberated after those bound to hydroxyl groups. Thus, the amino groups integrated into the TEPA-impregnated film retard the release of water molecules.

Sorption capacity tests

The immobilization of tetraethylenepentamine (TEPA) on the chitosan film crosslinked with 20% sodium citrate allows for an increase in the CO₂ sorption capacity by approximately 90.04% at room temperature, as shown in Figure 6, rising from 2.41 mmol CO₂/g for the unmodified membrane to 4.58 mmol CO₂/g for the impregnated film. Additionally, the increase in system temperature slightly enhances the CO₂ fixation capacity for the 20% crosslinked NaCit tetraethylenepentamine (TEPA)-loaded film with ($C_{CO_2} = 4.58$ mmol CO₂/g (room temp.), 4.97 mmol CO₂/g (50°C), and 5.92 mmol CO₂/g (80°C)), which can be attributed to the improvement in the CO₂ diffusion process into the impregnated surface liquid amine fraction, increasing accessibility to a greater number of active basic sites (see Figure 6). Therefore, when films are impregnated with a large amount of amines, diffusional effects can become more important than thermodynamic effects during the CO₂ sorption process.

On the other hand, the CO₂ capture capacity of 1% crosslinked NaCit films impregnated with tetraethylenepentamine (TEPA) remains relatively constant with increasing temperature ($C_{CO_2} = 3.01$ mmol

CO₂/g (room temp.), 3.42 mmol CO₂/g (50°C), and 3.30 mmol CO₂/g (80°C)).

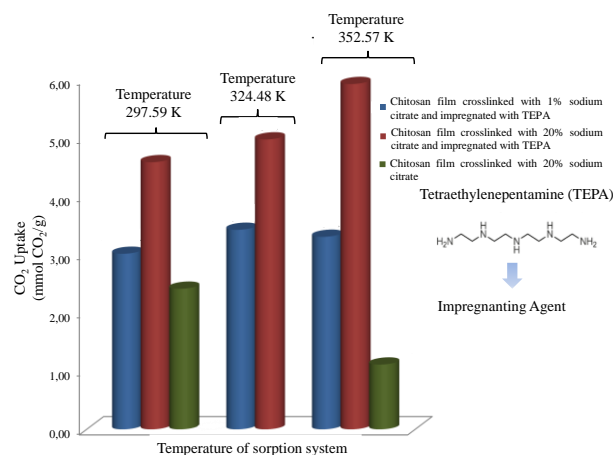


Fig. 6. CO₂ sorption capacity of chitosan films crosslinked with 1% and 20% sodium citrate and impregnated with tetraethylenepentamine (TEPA) at different temperatures ($T_1 = 297.59$ K, $T_2 = 324.48$ K, $T_3 = 352.57$ K)

The incorporation of basic sites into crosslinked films through impregnation with polyethylenimine (PEI) increased the CO₂ capture capacity by only 40.66% and 17.84% for films crosslinked with 1% and 20% NaCit, as shown in Figure 7. This improvement in sorption is attributed to the interactions between CO₂ and the basic nitrogen groups of the incorporated polyethyleneimine (PEI), resulting from Lewis acid-Lewis base electrostatic forces, leading to chemisorption of the sorbate. However, as the temperature increases, the sorption capacities tend to decrease from 3.39 mmol CO₂/g at room temperature to 2.54 mmol CO₂/g at 50°C and finally to 0.39 mmol CO₂/g at 80°C for the films crosslinked with 1% NaCit and impregnated with polyethyleneimine (PEI). This indicates the exothermic nature of the reaction between CO₂ and polyethyleneimine (PEI) and the notable thermodynamic effect on the sorption process.

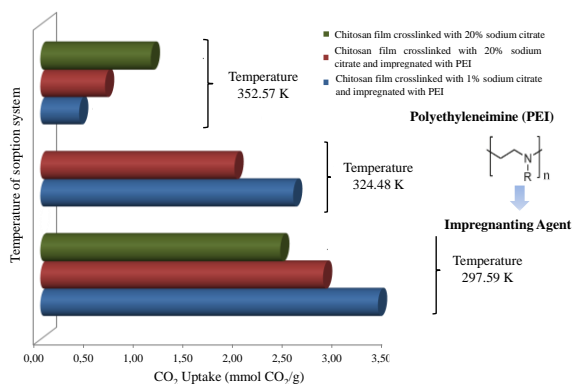
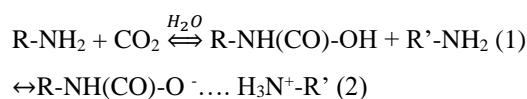


Fig. 7. CO₂ sorption capacity of chitosan films with 1% and 20% NaCit crosslinking and impregnated with polyethyleneimine at different temperatures (T₁ = 301.06 K, T₂ = 322.41 K, T₃ = 353.54 K).

Furthermore, the CO₂ adsorption capacities observed for TEPA-impregnated films exhibit a relative increase compared to those treated with PEI. Energy Dispersive X-ray Spectroscopy (EDX) analysis of both film (Figures 8b and 8c) illustrates a higher nitrogen content in the TEPA-loaded chitosan film, measuring at approximately 24.83%, in contrast to the PEI-loaded film with an approximate nitrogen content of 19.03% (compared to 6.87% for the untreated film, as shown in Figure 8a). This discrepancy in nitrogen content may elucidate, in part, the observed variations in CO₂ fixation capacities.

The interaction mechanism between basic groups and carbon dioxide is based in the reaction of primary amines of chitosan with CO₂ in the presence of water through a two-step sequence (1,2), forming a zwitterion, which can transfer a proton to an un-ionized amine to form the corresponding carbamate. A reaction sequence associated with this mechanism is:



Where the dashed line represents the ionic bond. The formation of the carbamate salt involves an acid-base equilibrium between carbamic acid and a secondary amine. As indicated by the reaction sequence, the formation of carbamic acid and carbamate salts is reversible.

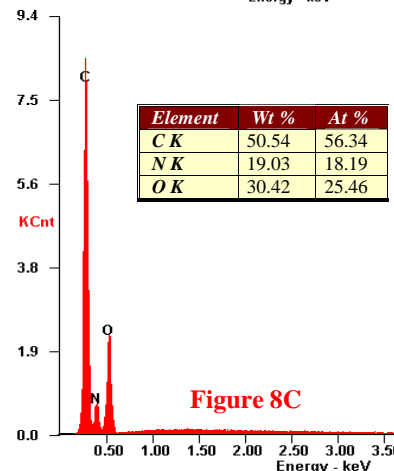
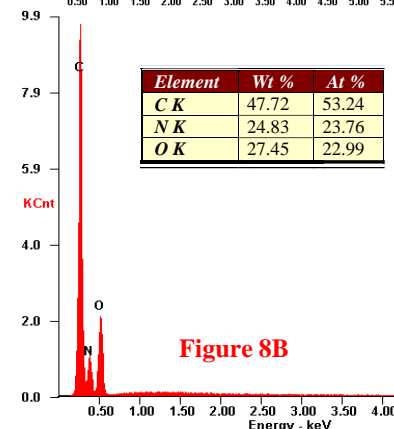
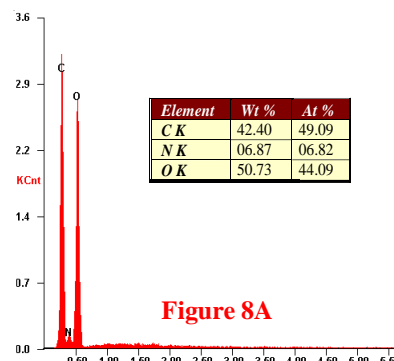


Fig. 8. Energy Dispersive X-ray Spectra of (a) 20% sodium citrate-crosslinked chitosan film; (b) tetraethylenepentamine-loaded chitosan film; (c) polyethylenimine-loaded chitosan film.

The monomeric glucopyranose unit of chitosan contains, besides the primary amino group, two hydroxyl groups—one on the ring and another on the hydroxymethyl group. These hydroxyl groups may play a role in stabilizing hydrogen bonds with CO₂ and, consequently, the sorption products. It is noteworthy that in absence of hydroxyl groups, the primary mechanism of CO₂ adsorption involves the formation of the zwitterionic carbamate, as described by reactions 1 and 2. In the presence of hydroxyl groups, the formation of this zwitterionic carbamate can be facilitated by the reaction (3):



The presence of free water and bound water in the three-dimensional network of the chitosan film facilitates the diffusion transport of CO₂ through the polymer matrix. Based on the thermogravimetric analysis of the membrane, an estimated content of free water of 8.74% and bound water of 5.23% was determined, resulting in a total water proportion of 13.97%. Both the free water, which exists in a separate phase within the polymer, and the bound water, which interacts via hydrogen bonds with hydrophilic groups of the network, allow for increased CO₂ permeation through the film. This is achieved through the formation of partial ionic charges that generate electrostatic interactions between the reactive primary amino groups of the chitosan polymer unit and the adsorbate (CO₂), creating a polarizing effect. This phenomenon facilitates diffusion transport through the film.

CONCLUSIONS.

In summary, the films subjected to crosslinking with sodium citrate undergo a change in surface topology, as verified by Scanning Electronic Microscopy (SEM). This

alteration in intramolecular order or short-range crystallinity conditions the existence of a denser and more regular structure at the microscopic level. The thermal degradation of chitosan occurs in three well-defined stages: (1) the first stage starts at 30°C and continues to 215°C, corresponding to the loss of water; (2) the second stage begins at 215°C and extends to 440°C, related to the thermal and oxidative decomposition of chitosan, as well as the vaporization and elimination of volatile products; and (3) the third thermal event (between 350 to 440°C) associated with the slow decomposition of the carbonaceous residue. The immobilization of basic groups through impregnation enhances CO₂ capture capacity. The temperature increase slightly enhances the CO₂ fixation capacity for films crosslinked with 20% NaCit and impregnated with tetraethylenepentamine (TEPA), which can be attributed to the improved diffusion process of CO₂ in the superficial liquid amine fraction, increasing accessibility to a greater number of basic active sites.

Finally, the following recommendations are provided for future work in this field: (a) increasing the surface area of chitosan films using lyophilization and porogen leaching methods with silica gel, allowing the development of a homogeneous porous structure conducive to the diffusion of CO₂ gas streams, and (b) selectivity studies with various types of pollutant gases, including CH₄, CO, H₂S, to achieve a high CO₂ removal capacity compared to other volumetric components of the combustion gas

REFERENCES

- [1] Masson-Delmotte, V., P. Zhai, A. Pirani, S.L. Connors, C. Péan, S. Berger, N. Caud, Y. Chen, L. Goldfarb, M.I. Gomis, M. Huang, K. Leitzell, E. Lonnoy, J.B.R. Matthews, T.K. Maycock, T. Waterfield, O. Yelekçi, R. Yu, and B. Zhou (2021). "Climate change 2021: the physical science

- basis. *Contribution of working group I to the sixth assessment report of the intergovernmental panel on climate change*". Cambridge University Press, Cambridge, United Kingdom and New York, NY, USA, 2(1), pp 2391.
- [2] Gulev, S. K., Thorne, P. W., Ahn, J., Dentener, F. J., Domingues, C. M., Gerland, S., Gong, D. S., Kaufman, S., Nnamchi, H. C., Quaas, J., Rivera, J. A., Sathyendranath, S., Smith, S. L., Trewin, B., von Shuckmann, K., and Vose, R. S. (2021). "Changing State of the Climate System, in: Climate Change 2021: The Physical Science Basis. *Contribution of Working Group I to the Sixth Assessment Report of the Intergovernmental Panel on Climate Change*". Cambridge University Press, Cambridge, United Kingdom and New York, NY, USA, 287–422.
- [3] Canadell, J. G., Monteiro, P. M. S., Costa, M. H., Cotrim da Cunha, L., Cox, P. M., Eliseev, A. V., Henson, S., Ishii, M., Jaccard, S., Koven, C., Lohila, A., Patra, P. K., Piao, S., Rogelj, J., Syampungani, S., Zaehle, S., and Zickfeld, K. (2021). "Global Carbon and other Biogeochemical Cycles and Feedback, in: Climate Change 2021: The Physical Science Basis, *Contribution of Working Group I to the Sixth Assessment Report of the Intergovernmental Panel on Climate Change*". Cambridge University Press, Cambridge, United Kingdom and New York, NY, USA, 673–816.
- [4] Friedlingstein, P., O'sullivan, M., Jones, M. W., Andrew, R. M., Bakker, D. C., Hauck, J., ... & Zheng, B. (2023). Global carbon budget 2023. *Earth System Science Data*, 15(12), 5301-5369.
- [5] Madejski, P., Chmiel, K., Subramanian, N., & Kuś, T. (2022). Methods and techniques for CO₂ capture: Review of potential solutions and applications in modern energy technologies. *Energies*, 15(3), 887.
- [6] Borgohain, R., Pattnaik, U., Prasad, B., & Mandal, B. (2021). A review on chitosan-based membranes for sustainable CO₂ separation applications: Mechanism, issues, and the way forward. *Carbohydrate Polymers*, 267, 118178.
- [7] Petroni, S., Tagliaro, I., Antonini, C., D'Arienzo, M., Orsini, S. F., Mano, J. F., Brancato, V., Borges, J., & Cipolla, L. (2023). Chitosan-based biomaterials: insights into chemistry, properties, devices, and their biomedical applications. *Marine drugs*, 21(3), 147.
- [8] Salehi, E., Daraei, P., & Shamsabadi, A. A. (2016). A review on chitosan-based adsorptive membranes. *Carbohydrate polymers*, 152, 419-432.
- [9] Balange, A. K., Layana, P., & Naidu, B. C. (2023). Harnessing value and sustainability: Fish waste valorization and the production of valuable byproducts. *Advances in Food and Nutrition Research*, 107, 175-192.
- [10] Morris, J. P., Backeljau, T., & Chapelle, G. (2019). Shells from aquaculture: a valuable biomaterial, not a nuisance waste product. *Reviews in Aquaculture*, 11(1), 42-57.
- [11] Cooney, R., de Sousa, D. B., Fernández-Ríos, A., Mellett, S., Rowan, N., Morse, A. P., Hayes, M., Laso, J., Rigueiro, L., Wan, A. H.L., & Clifford, E. (2023). A circular economy framework for seafood waste valorisation to meet challenges and opportunities for intensive production and sustainability. *Journal of Cleaner Production*, 392, 136283.
- [12] Ito, A., Sato, M., & Anma, T. (1997). Permeability of CO₂ through chitosan membrane swollen by water vapor in feed gas. *Die Angewandte Makromolekulare Chemie: Applied Macromolecular Chemistry and Physics*, 248(1), 85-94.
- [13] Kumar, S., De A. Silva, J., Wani, M. Y., Dias, C. M., & Sobral, A. J. (2016). Studies of carbon dioxide capture on porous chitosan derivative. *Journal of Dispersion Science and Technology*, 37(2), 155-158.
- [14] Rafigh, S. M., & Heydarinasab, A. (2017). Mesoporous chitosan–SiO₂ nanoparticles: synthesis,

- characterization, and CO₂ adsorption capacity. *ACS Sustainable Chemistry & Engineering*, 5(11), 10379-10386.
- [15] Kumar, S., Prasad, K., Gil, J. M., Sobral, A. J., & Koh, J. (2018). Mesoporous zeolite-chitosan composite for enhanced capture and catalytic activity in chemical fixation of CO₂. *Carbohydrate polymers*, 198, 401-406.
- [16] Prasad, B., & Mandal, B. (2017). CO₂ separation performance by chitosan /tetraethylenepentamine / poly (ether sulfone) composite membrane. *Journal of Applied Polymer Science*, 134 (34), 45206.
- [17] Francisco, G. J., Chakma, A., & Feng, X. (2010). Separation of carbon dioxide from nitrogen using diethanolamine-impregnated poly (vinyl alcohol) membranes. *Separation and Purification Technology*, 71(2), 205-213.
- [18] Ismail, A. F., Rahim, N. H., Mustafa, A., Matsuura, T., Ng, B. C., Abdullah, S., & Hashemifard, S. A. (2011). Gas separation performance of polyethersulfone/multi-walled carbon nanotubes mixed matrix membranes. *Separation and purification technology*, 80(1), 20-31.
- [19] El-Azzami, L. A., & Grulke, E. A. (2007). Dual mode model for mixed gas permeation of CO₂, H₂, and N₂ through a dry chitosan membrane. *Journal of Polymer Science Part B: Polymer Physics*, 45(18), 2620-2631.
- [20] El-Azzami, L. A., & Grulke, E. A. (2008). Carbon dioxide separation from hydrogen and nitrogen by fixed facilitated transport in swollen chitosan membranes. *Journal of Membrane Science*, 323(2), 225-234.
- [21] El-Azzami, L. A., & Grulke, E. A. (2009). Carbon dioxide separation from hydrogen and nitrogen: Facilitated transport in arginine salt-chitosan membranes. *Journal of Membrane Science*, 328(1-2), 15-22.
- [22] Silva, R.M., Silva G.A., Coutinho, O.P., Mano, J.F., Reis, R.L. (2004). Preparation and characterisation in simulated body conditions of glutaraldehyde crosslinked chitosan membranes. *J. Materials Sci.: Materials in Medicine*, 15(10), 1105-1112.
- [23] ASTM E1252-98(2021). Standard practice for general techniques for obtaining infrared spectra for qualitative analysis.
- [24] ASTM E1131-20. Standard test method for compositional analysis by thermogravimetry.
- [25] García, J.A., Castillo, L.A. (2005). Procedimiento para evaluar secuestrantes sólidos de gases ácidos en condiciones estáticas. *Manual Técnico. M-0432,2005*.
- [26] Nieto, J. M., Peniche-Covas, C., & Padro, G. (1991). Characterization of chitosan by pyrolysis-mass spectrometry, thermal analysis and differential scanning calorimetry. *Thermochimica acta*, 176, 63-68.
- [27] Hyun, D.; Jung, H.; Shin, D.; Lee, C.; Kim, S. (2014). Effect of amine structure on CO₂ adsorption over tetraethylenepentamine impregnated poly-methyl methacrylate supports. *Separation and Purification Technology*, 125, 187 – 193.